[CANCER RESEARCH 63, 2802–2811, June 1, 2003]

GTI-2040, an Antisense Agent Targeting the Small Subunit Component (R2) of Human Ribonucleotide Reductase, Shows Potent Antitumor Activity against a Variety of Tumors

Yoon Lee,[1] Aikaterini Vassilakos, Ningping Feng, Viengthong Lam, Hongsheng Xie, Ming Wang, Hongnan Jin, Keyong Xiong, Chenyi Liu, Jim Wright, and Aiping Young

Lorus Therapeutics Inc., Toronto, Ontario, M9W 4Z7 Canada

ABSTRACT

GTI-2040 is a 20-mer oligonucleotide that is complementary to a coding region in the mRNA of the R2 small subunit component of human ribonucleotide reductase. *In vitro* studies using a number of human tumor cell lines have demonstrated that GTI-2040 decreases mRNA and protein levels of R2 in a sequence- and target-specific manner. *In vivo* studies have shown that GTI-2040 significantly inhibits growth of human colon tumors (adenocarcinoma), pancreatic tumors (adenocarcinoma), liver tumors, lung tumors, breast tumors (adenocarcinoma), renal tumors, ovarian tumors (adenocarcinoma), melanoma, brain glioblastoma-astrocytoma, prostatic tumors, and cervical tumors in nude and/or severe combined immunodeficient mice. Antitumor effects were not observed with an oligonucleotide containing four mismatches to the *R2* sequence or with a scrambled sequence containing the same base content but not complementary to *R2*. This suggests that an antisense mechanism is responsible for the *in vivo* observations. In addition to tumor growth assays, GTI-2040 was tested in a murine model of human lymphoma. Treatment of severe combined immunodeficient mice bearing Burkitt's lymphoma with GTI-2040, but not control oligonucleotides, greatly extended the survival of mice, and survival extended well beyond the treatment period. Finally, GTI-2040 specifically inhibits metastasis of human melanoma cells to the lungs in nude mice. Taken together, the results of these studies indicate that GTI-2040 can act as a selective and specific anticancer agent against a broad range of human tumors.

INTRODUCTION

In 2002, 1,284,900 new cases of invasive cancer are expected to be diagnosed in the United States, and 555,500 people are expected to die from cancer (American Cancer Society Facts and Figures 2002).[2] Current therapeutic approaches to cancer include surgery, radiation, chemotherapy, and hormone and cytokine therapy. Each of these therapies has limited efficacy and can result in toxicity to normal cells. Thus, there is a need for therapies that specifically target tumor cells and therefore have more favorable safety profiles. Several therapeutic agents that inhibit RNR[3] as part of their mechanism of action are currently used. These include hydroxyurea [Hydrea (Bristol-Myers Squibb) and Hydroxyurea Capsules (Roxane)], gemcitabine (Gemzar; Eli Lilly), and fludarabine (Fludara; Berlex). Gemcitabine and fludarabine are not specific inhibitors of RNR, and treatment results in significant side effects that limit their effectiveness. Hydroxyurea is a reversible inhibitor of RNR that requires relatively high concentrations to be effective.

RNR catalyzes the reaction in which 2′-deoxyribonucleotides (dADP, dGDP, dUDP, and dCDP) are synthesized from the corresponding ribonucleoside 5′-diphosphates (ADP, GDP, UDP, and CDP). This step is the rate-limiting reaction in the production of 2′-deoxyribonucleoside 5′-triphosphates required for DNA replication (1). Human RNR consists of two protein components. R1 is a M_r 160,000 dimer that contains at least two different effector-binding sites, and R2 is a M_r 78,000 dimer that contains a non-heme iron that participates in catalysis by forming an unusual free radical on the aromatic ring of a tyrosine residue. Expression of both the *R1* and *R2* genes is required for enzymatic activity. Interestingly, *R1* and *R2* are encoded by different genes located on separate chromosomes, and the mRNAs are differentially expressed throughout the cell cycle (2, 3). Consequently, the level of R1 protein remains relatively stable throughout the cell cycle, whereas *R2* is only expressed during late G_1/early S phase, when DNA replication occurs. RNR activity is regulated by the amount of enzyme present in the cell and by allosteric control mechanisms involving positive and negative effectors (1, 4). In addition, *R2* expression appears to be regulated by a posttranslational mechanism in which the R2 protein half-life changes in response to cell cycle state (5). In murine cells, signal transduction via cyclic AMP, protein kinase C, and protein kinase A regulates RNR expression (6–9). Norepinephrine stimulation of differentiating adipocytes results in decreased expression of *R1* and *R2*. In contrast, norepinephrine stimulates *R2* but not *R1* expression in proliferating pre-adipocytes. The observed increase in expression was reduced by inhibition of Src and extracellular signal-regulated kinases 1/2, suggesting a role of these pathways in regulation of RNR activity in proliferating cells (9).

Recently, an *R2* paralogue, *p53R2*, was identified that is induced by DNA damage (10–12). Expression of *p53R2* is regulated by p53, via a p53 binding sequence in intron 1 of the *p53R2* gene. UV, γ-radiation, and Adriamycin treatment induce *p53R2* expression, but not *R2* expression, in a p53-dependent manner. In addition, p53R2 can form an active RNase reductase complex with R1, suggesting that R1 may be the endogenous partner of p53R2 (13). The identification of an alternate small subunit for the RNR complex may explain the previously observed differential expression of *R1* and *R2*. R2 appears to be responsible for the maintenance of dNTPs for replication, whereas p53R2 is responsible for production of dNTPs in response to DNA damage. Expression of *p53R2* is essential for DNA repair and as such represents a potential pathway for increasing sensitivity of cells to chemotherapeutic drugs (12).

Several recent studies provide renewed interest in targeting RNR in the development of anticancer therapeutics (14–18). An intriguing observation is that the retinoblastoma tumor suppressor suppresses *R1* and *R2* as one of the mechanisms by which it controls progression through the cell cycle (19). Retinoblastoma inactivation, often observed in tumors, leads to increased dNTP levels and a concomitant resistance of tumor cells to drugs such as 5-FU and hydroxyurea. The R2 protein also appears to play an additional role in determining the malignant potential of tumor cells via cooperation with a number of

Received 11/4/02; accepted 3/25/03.

The costs of publication of this article were defrayed in part by the payment of page charges. This article must therefore be hereby marked *advertisement* in accordance with 18 U.S.C. Section 1734 solely to indicate this fact.

[1] To whom requests for reprints should be addressed, at Lorus Therapeutics Inc., 2 Meridian Road, Toronto, Ontario, M9W 4Z7 Canada. Phone: (416) 798-1200; Fax: (416) 798-2200.

[2] www.cancer.org.

[3] The abbreviations used are: RNR, ribonucleotide reductase; ODN, oligodeoxynucleotide; AS-ODN, antisense oligodeoxynucleotide; SCID, severe combined immunodeficient; NK, natural killer; 5-FU, 5-fluorouracil; dNTP, deoxynucleoside triphosphate; FBS, fetal bovine serum; GAPDH, glyceraldehyde-3-phosphate dehydrogenase; HRP, horseradish peroxidase.

activated oncogenes. For example, anchorage-independent growth of cells transformed with v-*fms*, v-*src*, A-*raf*, v-*fes*, c-*myc*, and ornithine decarboxylase was significantly enhanced when R2 was overexpressed (20). Furthermore, overexpression of *R2* results in significant increases in membrane-associated Raf-1 protein and mitogen-activated protein kinase 2 activity, implicating a major Ras pathway in the Ras/R2 synergism (21). Increased expression of *R2* has been found to increase the drug resistant properties of cancer cells (22–24), whereas R2 expression in antisense orientation led to the reversal of drug resistance (22) and resulted in decreased proliferation of tumor cells (25). Recently, c-myc-dependent amplification and rearrangement of the *R2* gene were implicated in genome instability and potential neoplasia (26). Taken together, these studies indicate that, apart from the antiproliferative effect of RNR inhibition, the specific inhibition of *R2* expression would likely provide additional antineoplastic benefits.

AS-ODNs are currently being studied for their potential use as therapeutic agents for a variety of diseases including cancer (27–29). The gene-specific mechanism of action makes this class of compounds less toxic than conventional chemotherapeutic agents. In the present study, 102 AS-ODNs complementary to RNR subunit R2 were screened for the ability to decrease *R2* mRNA levels *in vitro*. One AS-ODN, GTI-2040, was further characterized in *in vivo* assays for antitumor activity. The results presented here provide evidence that GTI-2040 acts in a specific, dose-dependent manner to downregulate *R2* expression with a concomitant decrease in tumor growth and metastasis and an increase in animal survival. Given these data, GTI-2040 shows promise as an antitumor drug candidate.

MATERIALS AND METHODS

ODN Synthesis. Phosphorothioate nucleotides have one of the nonbridging oxygen molecules replaced with a sulfur atom. The resultant phosphorothioate ODN structure provides increased resistance to degradation by nucleases, thereby increasing *in vivo* stability (30, 31). All ODNs used in this study were fully thioated. They were synthesized on an automated DNA synthesizer (Perkin-Elmer) by Boston BioSystem Inc. (Boston, MA). ODNs were purified, and purity was assessed by reversed-phase high performance liquid chromatography. Each ODN preparation was found to contain >95% full-length material. GTI-2040 hybridizes to the coding region of *R2* mRNA, and its sequence is 5′-GGCTAAATCGCTCCACCAAG-3′ (Fig. 1). A mismatched control analogue of GTI-2040, named GTI-2040mismatched (5′-GGCTAAACTCGTCCACCAAG-3′), contains four base changes in the middle of GTI-2040 sequence. A scrambled control analogue of GTI-2040, GTI-2040scrambled (5′-ACGCACTCAGCTAGTGACAC-3′), is not complementary to *R2* but retains the same base composition ratio.

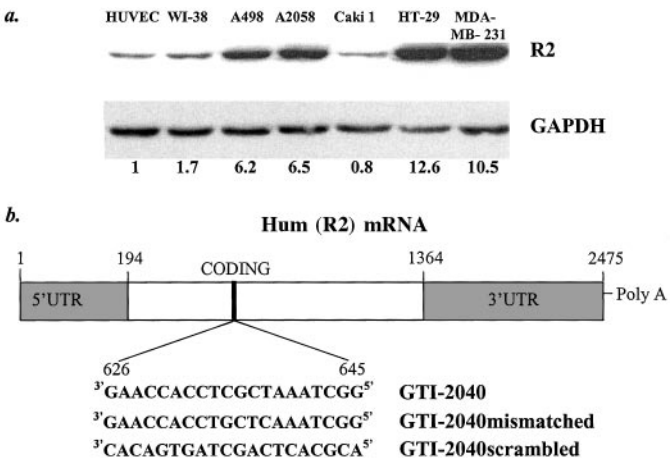

Fig. 1. *a*, cell lines were grown to 80% confluency, cell lysates were prepared in radioimmunoprecipitation assay buffer, and equal amounts of protein were resolved by SDS-PAGE, followed by Western blot analysis with antibodies specific for R2 (*top panel*) and GAPDH (*bottom panel*). The relative level of R2 in the different cell lines, assessed by densitometric analysis to produce a R2:GAPDH ratio, is shown *below* each lane. *b*, *R2* mRNA schematic with GTI-2040 target region and sequence of GTI-2040, GTI-2040mismatched, and GTI-2040scrambled.

Cell Lines and Cell Culture. Unless noted otherwise in the text, human tumor cell lines were purchased from American Type Culture Collection (Manassas, VA). Human colon adenocarcinoma (HT-29), non-small cell lung carcinoma (NCI-H460), melanoma (A2058), breast adenocarcinoma (MDA-MB-231), pancreatic carcinoma (AsPC-1 and SU.86.86), glioblastoma-astrocytoma (U-87 MG), renal carcinoma (A498 and Caki-1), ovarian carcinoma (SK-OV-3), cervical carcinoma (HeLa S3), prostate carcinoma (PC-3), bladder carcinoma (T24), Burkitt's lymphoma (Raji), and hepatocellular carcinoma (Hep G2) were maintained, according to American Type Culture Collection recommendation, in α-MEM, RPMI 1640, or McCoy's 5a medium (Invitrogen Canada Inc., Burlington, Ontario, Canada) supplemented with 10–20% FCS at 37°C in a humidified atmosphere containing 5% CO_2. Normal human cell lines, WI-38 (human lung fibroblast), human umbilical vein endothelial cells, and murine R3 (fibrosarcoma) and L (Ltk$^-$ fibroblast) cells were maintained as mentioned above. C8161 metastatic melanoma cells were a gift from Dr. D. R. Welch (University of Pennsylvania, Hershey, PA) and were maintained as described above (32). All media used in these experiments contain an antibiotic-antimycotic solution at a final concentration of 100 units/ml penicillin and 100 μg/ml streptomycin (Invitrogen Canada Inc.).

ODN Treatment of the Cells in Culture. Aliquots of cell suspension were seeded into 60- or 100-mm tissue culture dishes and grown in appropriate media to subconfluence (75–85%). At this time, the cells were washed once with PBS (pH 7.2) and treated with 0.2 μM ODN, unless noted otherwise, in the presence of cationic lipid [Lipofectin reagent and a final concentration of 5 μg/ml DOTMA/DOPE (Invitrogen Canada Inc.)] for 4 h. After the incubation period, the media containing ODNs were removed, and cells were washed once with PBS. The cells were then cultured in growth medium for the duration indicated in the text.

Measurement of R2 Protein Levels. To measure the effect of GTI-2040 on R2 protein levels, Western blot analysis was conducted as described previously (21, 33), with minor modifications. Briefly, cells were treated with ODNs for 4 h, incubated for 8–18 h, and washed once with PBS, and whole cell protein extracts were prepared in 50–150 μl of 2× sample loading buffer [100 mM Tris (pH 6.8), 200 mM DTT, 4% SDS, 20% glycerol, and 0.015% bromphenol blue]. Extracted protein (10–20 μg) was fractionated on 12% SDS-PAGE and transferred to nitrocellulose or polyvinylidene difluoride membranes, and total protein was visualized by India ink staining. The R2 protein was detected with an anti-R2 polyclonal antibody, followed by a HRP-conjugated secondary antibody, and the M_r 45,000 R2 protein was visualized by ECL (Amersham, Arlington Heights, IL). Three R2-specific antibodies were used: one rabbit antimouse antibody (34, 35) and two goat antihuman R2 antibodies (Santa Cruz Biotechnology). Where indicated, the blots were probed for GAPDH protein as a loading control (mouse anti-GAPDH monoclonal antibody; Biodesign International). The secondary antibodies were as follows: HRP-conjugated antigoat IgG (Sigma) and HRP-conjugated donkey antimouse (Santa Cruz Biotechnology).

Immunoprecipitation was performed using saturating amounts of antimouse R2 polyclonal antibody as described previously (33, 35). Briefly, cells were treated as described above, washed with PBS, and labeled with [^{35}S]methionine for 4–7 h, and cell extracts were prepared by lysis in SB250 buffer [250 mM NaCl, 25 mM Tris-HCl (pH 7.5), 5 mM EDTA, 1% Triton X-100, and 0.5% sodium deoxycholate]. R2 protein was specifically immunoprecipitated by incubation with saturating amounts of R2 antibody followed by incubation with formalin-fixed *Staphylococcus aureus* cells (Pansorbin; Calbiochem). The isolated protein was resolved on 12% SDS-PAGE and visualized by autoradiography.

Measurement of R2 mRNA Levels. To measure the effect of GTI-2040 on *R2* mRNA levels, Northern blot analysis was conducted as described previously (36), with minor modifications. Briefly, cells were treated as described above, and total cellular RNA was prepared using Trizol reagent (Invitrogen Canada Inc.). Total cellular RNA (10–20 μg) was resolved on a 1.0% denaturing formaldehyde-agarose gel and transferred to nylon membrane using capillary transfer method. The blots were hybridized with a ^{32}P-labeled probe generated from the cDNA of R2 (37). Probes were labeled by random primer extension. Human *R2* mRNA was expressed as two bands, 3.4 and 1.6 kb

transcripts, presumably due to alternative polyadenylation (38–40) and was visualized and quantified using autoradiography or PhosphorImager analysis (Molecular Dynamics, Sunnyvale, CA). Either *GAPDH* mRNA or RNase levels were simultaneously probed or stained with methylene blue, respectively, for RNA loading controls.

***In Vivo* Treatment with AS-ODNs.** CD-1 athymic female nude mice, BALB/c *nu/nu* nude mice, SCID mice, and SCID beige mice were purchased from Charles River Laboratories (Montreal, Quebec, Canada), and experiments were typically initiated when the mice were 6–7 weeks old. Human tumor cells were grown in appropriate growth medium, and 3×10^6 to 1×10^7 cells suspended in 100 μl of PBS were s.c. injected into the right flank of the animals with a 23-gauge needle (cell number is indicated in the figure legends). Each experimental group typically contained 10 mice. After the size of tumor reached a mean tumor volume of 50–100 mm^3, treatment was initiated. AS-ODNs (dissolved in saline) were administered by bolus infusion into the tail vein of animal every other day at the indicated dose. Treatment with 5-FU (Pharmacia), vinblastine (Faulding), and gemcitabine (Eli Lilly) was as indicated in the figure legend. Antitumor activity was estimated by the measurement of tumor volume with a caliper at 2–3-day intervals. Tumor volume was calculated by a formula $L \times W \times H/2$, where L indicates length, W indicates width, and H indicates height. Within 24 h after the last treatment, the animals were sacrificed, and tumor and body weights were measured. Results of statistical analyses of the data are presented as Ps in the figure legends. To measure the changes in the expression of *R2* mRNA in tumors, excised tumor fragments were immediately collected into Trizol reagent (Invitrogen Canada Inc.) for mRNA extraction according to the manufacturer's protocol. Northern blot analysis was conducted as described above.

To determine R2 protein levels, protein was extracted from excised tumors (a maximum of 2 samples/treatment group). Briefly, whole cell protein extracts from tumor samples were prepared in 0.5 ml of radioimmunoprecipitation assay extraction buffer [50 mM Tris-HCl (pH 7.5), 150 mM NaCl, 1% NP40, 0.5% sodium deoxycholate, 0.1% SDS, 0.02% NaN_3, 1 mM phenylmethylsulfonyl fluoride, and 10 μM leupeptin] by rapid homogenization. Protein concentration was determined by Bio-Rad protein assay according to the manufacturer's protocol. Equivalent amounts of protein were heated in sample buffer at 100°C for 5 min, resolved by 12% SDS-PAGE, and transferred to nitrocellulose or polyvinylidene difluoride membrane. R2 protein was detected as mentioned above. If tumor regression occurred, mRNA and protein were isolated from spleen tissue instead of from tumors (*i.e.*, A498 tumors).

Lymphoma Survival Assay. Viable human Burkitt's lymphoma (Raji) cells (5×10^6) collected from subconfluent logarithmically growing cultures were injected i.v. into SCID mice, via the tail vein of each animal, and disease was allowed to establish for 2 days. ODNs, in normal saline, were administered by tail vein injections every second day at a dose of 10 mg/kg. Control animals received saline alone, without ODN or with mismatched and scrambled control ODNs. Each treatment group typically contained 10 animals. Treatment with ODN was stopped as indicated in the figure legend. The antitumor efficacy of treatment was assessed by the examination of the survival of the mice. Survival is reported as a percentage of the starting number of mice in the treatment group.

Experimental Metastasis Assay. C8161 human melanoma cells were seeded into 100-mm tissue culture dishes at a density of 2×10^6 cells/dish and incubated overnight at 37°C in α-MEM supplemented with 10% FBS. The cells were trypsinized and collected by centrifugation, and aliquots were removed from the suspension to determine the cell viability using the trypan blue exclusion test. Approximately 1×10^5 cells suspended in 0.1 ml of PBS were injected into the tail vein of 6–8-week old CD-1 athymic female nude mice. Treatment, as indicated in the figure legend, was initiated after 2 days. Estimates of the number of lung nodules were made 5–7 weeks later, after excised lungs from individual mice were stained with picric acid dye solution (75% picric acid, 20% formaldehyde, and 5% glacial acetic acid).

Densitometry. Results were quantified using Bio-Rad GelDoc System and Bio-Rad Quantity One quantitation software (version 4.3.0).

RESULTS

R2 Protein Levels Are Elevated in Cancer Cell Lines. Earlier studies have demonstrated elevated RNR levels and activity in tumors and tumor cell lines (41–43). To assess whether this is a general phenomenon of cancer cells, the R2 protein levels were examined in normal cell lines and cancer cell lines derived from diverse cancer types (Fig. 1*a*). Consistent with its role in cancer progression, R2 levels were elevated in four of five of the cancer cell lines. The increase in R2 varied from 6- to 12-fold compared with the level of R2 in human umbilical vein endothelial cells and from 3.6- to 7-fold compared with R2 levels in WI-38 cells. Caki-1 cells were the only exception, and R2 levels in these cells were decreased compared with those in both normal cell lines. This was not unexpected, given that Caki-1 cells appear to have a reduced growth rate compared with those of other tumor cell lines *in vitro*.[4]

Screening of Antisense Compounds to RNR *R2*. In all, 102 AS-ODNs were designed that span the 5′-untranslated region, coding region, and 3′-untranslated region of *R2* mRNA. Initially, the ODNs were screened for the ability to prevent proliferation and decrease *R2* mRNA in cancer cells *in vitro* (data not shown). In total, 30 promising candidate ODNs were chosen for further analysis *in vivo*. Of these, 18 compounds demonstrated varying antitumor activity against one or more human cancer xenografts in mice. Based on consistent target down-regulation, antiproliferative activity, and antitumor efficacy, GTI-2040 was chosen as a lead compound for further development. The region in *R2* that is complementary to GTI-2040 is shown in Fig. 1*b* along with the sequences of GTI-2040mismatched and GTI-2040scrambled, ODNs that act as controls for non-sequence-specific effects of GTI-2040. These controls are necessary, given that phosphorothioate-modified ODNs can be bioactive independent of antisense target binding (44). The region targeted by GTI-2040 is identical in rat, monkey, mouse, and human.[5] Given the sequence conservation, GTI-2040 efficacy and toxicity could be evaluated in a number of animal models.

GTI-2040 Specifically Inhibits Expression of R2 mRNA and Protein in a Number of Cell Lines. As a measure of the broad applicability of GTI-2040 as an antisense compound, its ability to down-regulate the target mRNA and, subsequently, protein synthesis was assessed *in vitro* in a number of cell types (Fig. 2, *a–c*) and *in vivo* (Fig. 3). In human NCI-H460 cells, *R2* mRNA levels decrease significantly after a 4-h exposure to GTI-2040 followed by an 18-h incubation, whereas the GTI-2040mismatched control sequence does not down-regulate *R2* mRNA (Fig. 2*a*). The decrease in mRNA corresponds to a decrease in both the steady-state level (Western blot in Fig. 2*b*, Mouse L cells) and biosynthetic rate (Fig. 2*c*, [^{35}S]methionine labeling of human T24 bladder carcinoma cells) of R2 protein. These changes were observed in a broad number of cell types, both human and murine (data not shown). It is interesting to note that R2 protein levels return to normal within 72 h after GTI-2040 treatment (Fig. 2*d*). R2 protein levels were determined from tumors or spleens (as indicated) excised from mice after treatment with GTI-2040. Consistent with GTI-2040 functioning via an antisense mechanism, treatment with GTI-2040 resulted in down-regulation of *R2* mRNA and protein (Fig. 3, *a* and *b*, respectively). Consistent with sequence-specific activity, the scrambled control oligonucleotide did not down-regulate R2 protein expression (Fig. 3*b*).

In A2058 cells, the effect of GTI-2040 on several endogenous RNAs was assessed by Northern blot analysis (Fig. 4). *R2* mRNA levels were down-regulated by GTI-2040, but not by the scrambled control, suggesting that the mechanism of down-regulation is sequence specific. RNA levels of *β-actin*, *signal recognition particle*, *RNase P*, and others did not decrease after GTI-2040 treatment,

[4] Y. Lee and A. Vassilakos, unpublished observations.

[5] E. S. Ferdinandi, A. Vassilakos, D. P. Fitsialos, A. H. Young, M. Adamo, M. Blaquire, P. Noonan, J. A. Wright. Preclinical toxicity and toxicokinetics of GTI-2040, a novel phosphorothioate oligonucleotide targeting ribonucleotide reductase R2, manuscript in preparation.

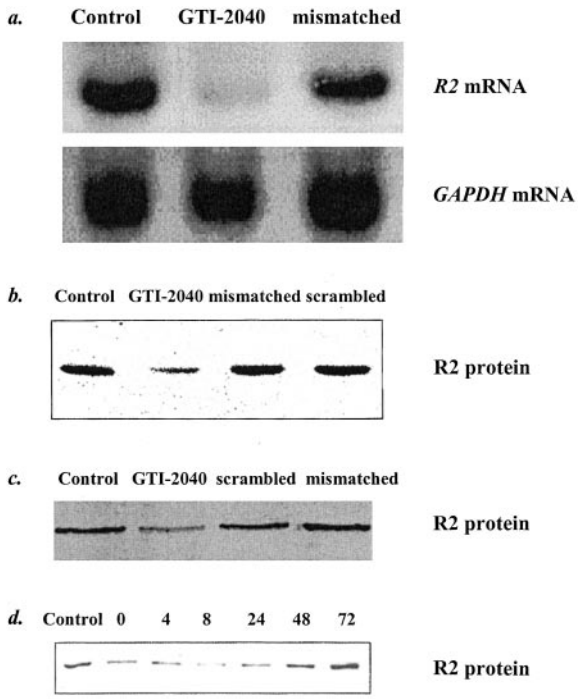

Fig. 2. *In vitro* Lipofectin-mediated transfection of a number of human and murine cell lines with 0.2 μM GTI-2040, GTI-2040mismatched, and GTI-2040scrambled. Cells were treated for 4 h, washed, and subsequently incubated for 10–24 h (except *c*) in fresh media. *a*, human NCI-H460 lung carcinoma cells. *R2* mRNA was determined by Northern blot analysis. In this figure, the larger 3.4-kb transcript of R2 is shown. GAPDH is shown in the *bottom panel* as a loading control. *b*, murine L cells. Steady-state levels of R2 protein were determined by Western blotting after treatment with Lipofectin alone (*Control*), GTI-2040, GTI-2040mismatched, or GTI-2040scrambled. *c*, human T24 bladder cancer cells. Biosynthetic rate of R2 was measured after GTI-2040 treatment. Cells were treated with Lipofectin alone (*Control*), GTI-2040, GTI-2040mismatched, or GTI-2040scrambled; washed; and radiolabeled for 4 h with [^{35}S]methionine. R2 synthesis was assessed by immunoprecipitation. *d*, murine L cells. Steady-state levels of R2 protein were determined by Western blotting at the indicated times (in hours) after GTI-2040 treatment. Control cells were treated with Lipofectin alone.

suggesting that GTI-2040 specifically targets *R2* mRNA (Fig. 4). Taken together, these results suggest a highly target-selective mechanism of action. As a component of RNR, it is expected that down-regulation of *R2* will result in arrest of cell proliferation. Consistent with a role for R2 in DNA replication and ultimately in cell proliferation, GTI-2040 displays high antiproliferative activity in colony-forming assays *in vitro* against a broad range of tumor cell types (data not shown). Proliferation was dose-dependent and saturable, with maximal effect occurring at 0.2 μM (data not shown).

GTI-2040 Displays Sequence-specific and Dose-dependent Antitumor Activity *in Vivo*. To determine whether GTI-2040 has antitumor activity, murine R3 fibrosarcoma or human Caki-1 and A498 cells were injected into mice, and tumors were allowed to grow until they were palpable and could be measured accurately with calipers. Subsequently, mice were treated with saline, GTI-2040, or control ODNs, and tumor growth was assessed by measurement of volume over time (Fig. 5*a* and Fig. 6, *a* and *c*) or of tumor weight at the end point of the experiment (Fig. 5*b* and Fig. 6, *b* and *d*). GTI-2040 had significant antitumor activity against all three tumor types. Furthermore, the mismatched and scrambled control ODNs had no antitumor activity, suggesting that the effect with GTI-2040 is sequence-specific. Similar sequence-specific antitumor activity was observed with human HepG2 tumor xenografts (data not shown). Finally, GTI-2040 demonstrates dose-dependent antitumor activity against both murine (R3) and human tumors (HT-29; Fig. 5*c*; data not shown).

Consistent with a RNR having a general role in tumor growth, GTI-2040 displays antitumor activity against a wide range of solid tumors *in vivo*. Fig. 7 summarizes the results of a statistical analysis of data compiled from a number of experiments in which the effect of GTI-2040 on tumor growth was assessed in human tumor cell xenografts in mice. Unlike examples of antisense compounds developed against specific tumors (*e.g.*, Bcl-2), GTI-2040 appears to be active against a range of cancer types. In all cancer cell lines tested, GTI-2040 treatment resulted in a significant decrease in tumor growth (volume over time; data not shown) and end point weight (Fig. 7). Interestingly, GTI-2040 has exceptional efficacy against renal cell carcinomas. GTI-2040 treatment results in dramatic growth inhibition of Caki-1 renal tumors as assessed by both tumor volume and tumor weight at the experimental end point (Fig. 6, *a* and *b*, respectively). Treatment resulted in a rapid tumor stabilization and shrinkage within the first week of treatment (Fig. 6, *a* and *b*). Tumor regression was complete within 3 weeks of treatment (day 28 after implantation of tumor). At the same dose, treatment with the control ODNs resulted in tumor growth that was indistinguishable from saline treatment. The results with A498 tumor xenografts were equally impressive, with complete tumor regression by day 33 (Fig. 6, *c* and *d*).

GTI-2040 Has Superior Antitumor Efficacy Compared with RNR-based Therapeutic Compounds. To assess the clinical potential of GTI-2040, its efficacy against human tumor cell xenografts in mice was compared with that of 5-FU, gemcitabine, and vinblastine (Fig. 6). These compounds are currently in clinical use and are thought to act, at least partially, by decreasing RNR activity. Without exception, GTI-2040 was superior to any of these compounds against two human renal tumors, Caki-1 and A498 tumors (Fig. 6). In addition, GTI-2040 was the only compound that displayed long-term protection from tumor growth. In A498 tumor xenografts, 5-FU, gemcitabine, and vinblastine treatments were all ineffective in stabilization of the tumors. By day 54, mice treated with 5-FU had tumors that were equal in volume and weight to tumors of saline-treated

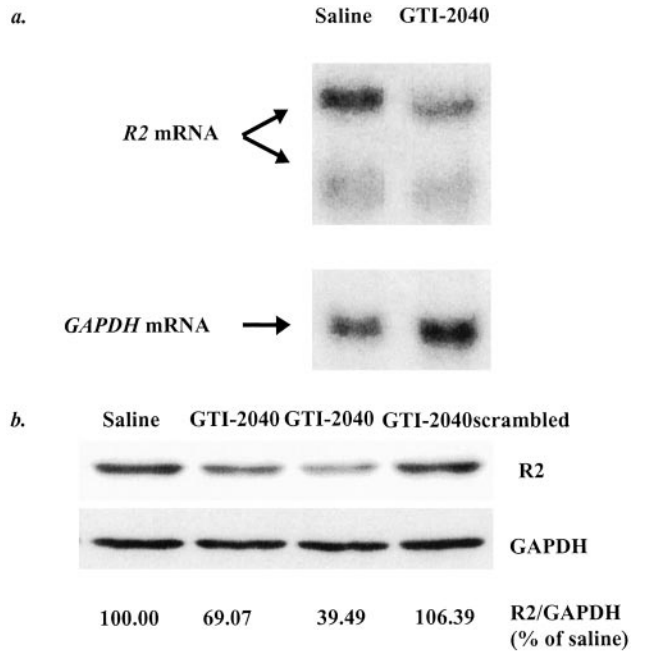

Fig. 3. *a*, total RNA was extracted from R3 tumors excised from mice treated with saline or GTI-2040 and subjected to Northern blot analysis probing for *R2* (*top panel*) and *GAPDH* (*bottom panel*; loading control). *b*, Western blot analysis of protein extracted from spleens excised from mice bearing A498 xenografts. Mice were treated with saline, GTI-2040, and GTI-2040scrambled as indicated. Equal amounts of protein were loaded in each lane, and blots were stained to ensure proper loading. R2 protein is shown, and GAPDH was used as a loading control. Densitometric analysis of expression is shown *below* each lane. The results were corrected for loading by expressing the results as the percentage of R2:GAPDH compared with saline (100%).

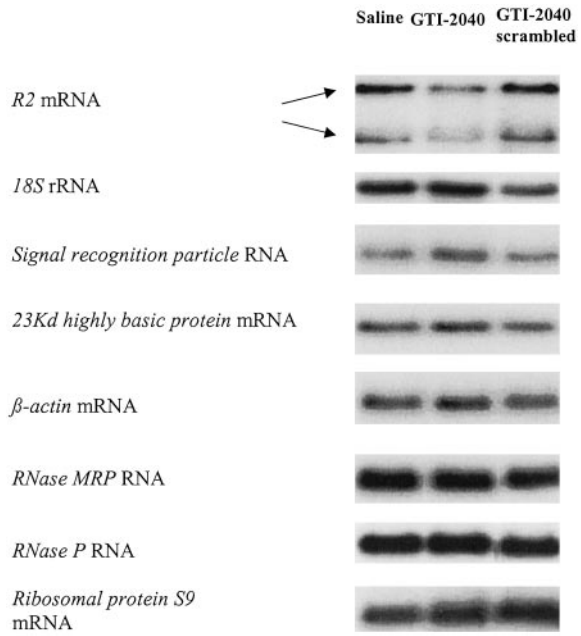

Fig. 4. A2058 human melanoma cells, grown to subconfluence (70–80%), were treated with 0.2 μM ODNs for 4 h in the presence of cationic lipid and OPTI-MEM I. Cells were washed once with PBS and incubated for 16 h in α-MEM containing 10% FBS. Total RNA was prepared in Trizol reagent, and Northern blot analysis was performed. The blots were hybridized with ^{32}P-labeled probes that detect *R2* mRNA, *18S* rRNA, *signal recognition particle* RNA, *23kDa highly basic protein* mRNA, *β-actin* mRNA, *MRP* RNA, *RNase P* RNA, and *ribosomal protein S9* mRNA.

animals. Whereas vinblastine and gemcitabine displayed better efficacy than 5-FU, there was, at best, a delay in the rate of tumor growth (Fig. 6*c*). These results are significant in that GTI-2040 is the only RNR-based compound developed to date that is highly specific for its target, thereby decreasing the potential for toxicity. 5-FU, gemcitabine, and vinblastine are highly toxic, and in most cases, long-term treatment with these compounds leads to drug resistance and subsequent tumor regrowth (45).

GTI-2040 Treatment Dramatically Prolongs Survival in Xenograft Model. As an additional test of efficacy, GTI-2040 was administered to SCID mice bearing active Burkitt's lymphoma (Fig. 8). GTI-2040 treatment leads to a dramatic increase in survival time of mice well beyond the treatment period (up to 72 days after the end of treatment; data not shown). In addition to prolonged survival, the GTI-2040-treated mice appeared to recover from the symptoms associated with the lymphoma. As treatment progressed, the GTI-2040-treated mice changed from having rough coats and weight loss to smooth coats and weight gain. Although strictly qualitative, these observations would suggest that the disease is not only stabilizing but also regressing, consistent with the prolonged survival after the end of treatment. Finally, neither scrambled nor mismatched control ODNs prolonged survival, consistent with GTI-2040 acting via a sequence-specific mechanism. Survival assays were carried out with mouse erythroleukemia cells as the inoculating cancer cell, with similar results (data not shown).

GTI-2040 Treatment Dramatically Decreases Lung Nodule Formation in an Experimental Metastasis Model. Murine R3 fibrosarcoma and human C8161 melanoma cells injected into the tail vein of mice form observable lung nodules 2 weeks after injection. Pretreatment of these tumor cells with 0.2 μM GTI-2040 in culture, before injection into mice, significantly reduces the extent of lung nodule formation (data not shown). To more accurately reflect the clinical situation, mice were treated with GTI-2040 after tumor cell injection. Under these conditions, GTI-2040 dramatically reduced the number of observed lung nodules compared with the saline treatment group (Fig. 9). As with the tumor and survival assays, there was no antimetastatic activity associated with treatment with control ODNs (Fig. 9, GTI-2040mismatched and GTI-2040scrambled), again confirming the sequence-specific effect of GTI-2040.

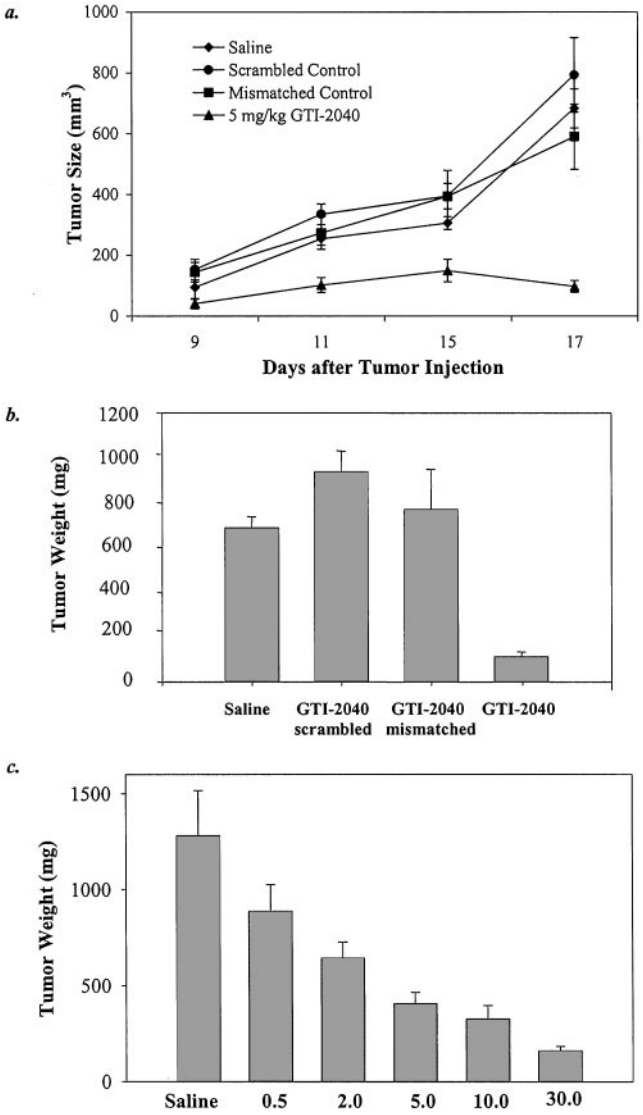

Fig. 5. R3 mouse fibrosarcoma cells (1.5×10^6 cells in 100 μl of PBS) were s.c. injected into the right flank of 6–8-week-old C3H female mice. After the tumor size reached an approximate volume of 100 mm^3, 3 days after tumor cell injection, GTI-2040, GTI-2040mismatched, and GTI-2040scrambled were administered by bolus infusion into the tail vein every other day at 5 mg/kg. Control animals received saline alone for the same period. Treatments lasted for 14 days thereafter. *a*, antitumor activities were estimated by the inhibition of tumor volume, which was measured with a caliper at 2-day intervals starting on day 9. Each *point* represents the mean tumor volume calculated from 6–7 animals/experimental group. The GTI-2040 treatment had significant antitumor efficacy compared with saline, scrambled, and mismatched controls ($P = 0.0001$) *b*, mean weight of tumors excised from the above-mentioned animals at the end of treatment. GTI-2040 had significant antitumor activity compared with saline ($P = 0.0006$), scrambled ($P = 0.0001$), and mismatched (0.0002) controls *c*, R3 mouse fibrosarcoma cells (2×10^6 cells in 100 μl of PBS) were s.c. injected into the right flank of 6-week-old C3H female mice. After the tumor size reached an approximate volume of 100 mm^3, 4 days after tumor cell injection, increasing concentrations (0.5–30 mg/kg, designated as *0.5–30*) of GTI-2040 were administered by bolus infusion into the tail vein every other day for 10 days. Control animals received saline alone for the same period. At the end of the treatments, the animals were sacrificed, tumors were excised, and their weights were measured. Each *bar* represents mean tumor weight and SE calculated from 6–8 animals/experimental group. *P*s compared with saline were as follows: 0.5 mg/kg, $P = 0.04$; 2 mg/kg, $P = 0.0001$; 5 mg/kg, $P = 0.0015$; 10 mg/kg, $P = 0.0001$; and 30 mg/kg, $P = 0.0001$.

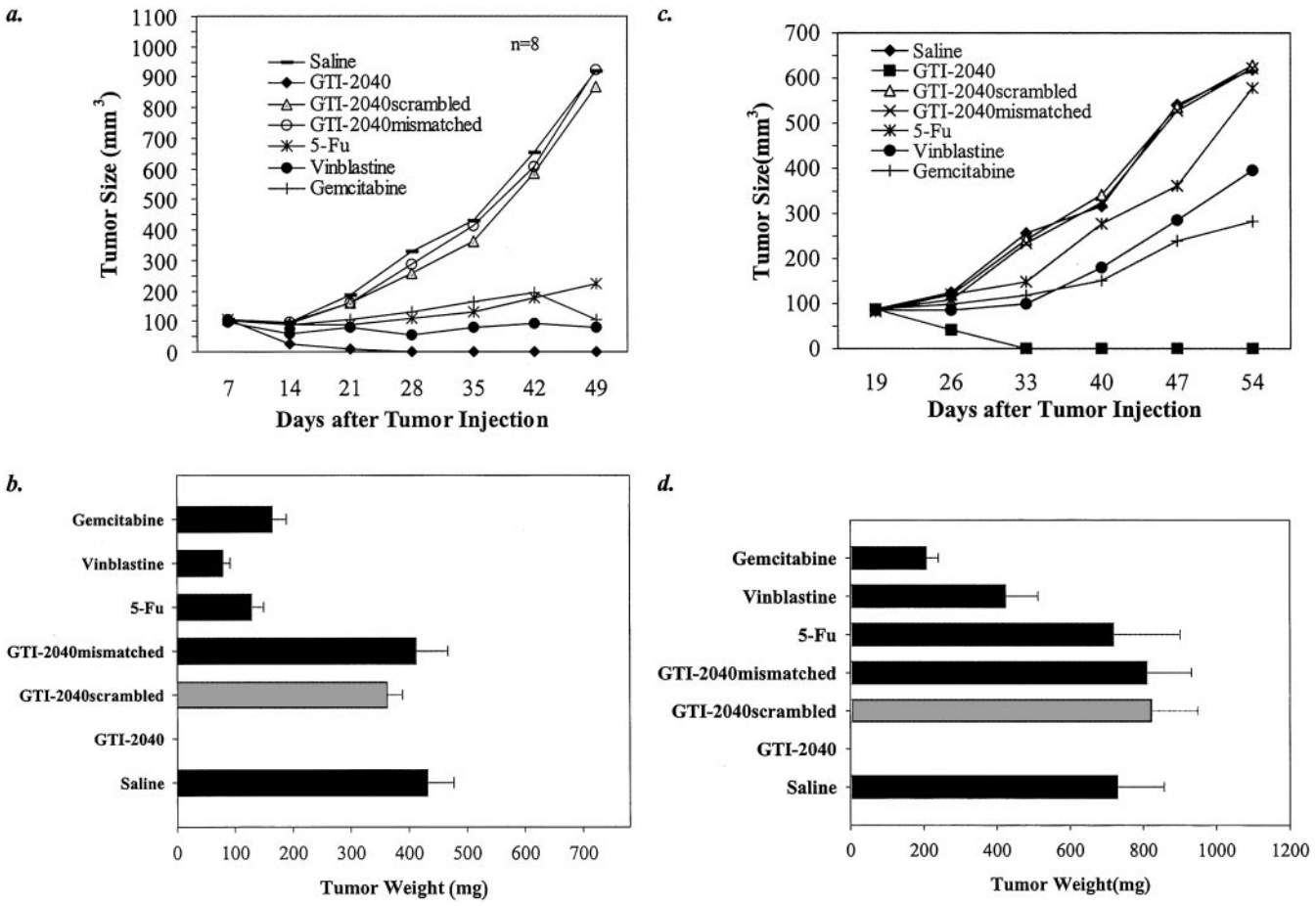

Fig. 6. *a*, Caki-1 human kidney cancer cells (5×10^6 cells in 100 μl of PBS) were s.c. injected into the right flank of 6–7-week-old female SCID mice. After the tumor size reached an approximate volume of 100 mm^3, 7 days after tumor cell injection, GTI-2040, GTI-2040mismatched, or GTI-2040scrambled was administered (10 mg/kg/2 days, i.v.). Three additional treatment groups received 5-FU (13 mg/kg/day $\times$ 5), vinblastine (1 mg/kg/week), and gemcitabine (100 mg/kg/week). Control animals received saline alone for the same period. Caliper measurements at 1-week intervals were used to calculate tumor volumes. Each *point* represents mean tumor volume calculated from 10 animals/experimental group (with the exception of GTI-2040, which was calculated from 8 animals). *P*s compared with saline: GTI-2040, $P < 0.0001$; scrambled, $P = 0.4032$; mismatched, $P = 0.8555$; 5-FU, $P < 0.0001$; vinblastine, $P < 0.0001$; and gemcitabine, $P < 0.0001$. *b*, after 49 days, the mice were sacrificed, and the tumors were weighed. Each *bar* represents the mean tumor weight and SE calculated for each treatment group. *P*s compared with saline: GTI-2040, $P = 0.0001$; scrambled, $P = 0.7183$; mismatched, $P = 0.3254$; 5-FU, $P = 0.0002$; vinblastine, $P = 0.0001$; and gemcitabine, $P = 0.0007$. *c*, A498 human kidney cancer cells (5×10^6 cells in 100 μl of PBS) were s.c. injected into the right flank of 6–7-week-old female SCID mice. After the tumor size reached an approximate volume of 100 mm^3, 19 days after tumor cell injection, GTI-2040, GTI-2040mismatched, or GTI-2040scrambled was administered (10 mg/kg/2 days, i.v.). Three additional treatment groups received 5-FU (13 mg/kg/day $\times$ 5), vinblastine (1 mg/kg/week), and gemcitabine (100 mg/kg/week). Control animals received saline alone for the same period. Caliper measurements at 1-week intervals were used to calculate tumor volumes. Each *point* represents mean tumor volume calculated from 10 animals/experimental group (with the exception of GTI2040, which was calculated from 8 animals). *P*s compared with saline: GTI-2040, $P = 0.0001$; scrambled, $P = 0.8786$; mismatched, $P = 0.8224$; 5-FU, $P = 0.8826$; vinblastine, $P < 0.0001$; and gemcitabine, $P < 0.0001$. *d*, after 54 days, the mice were sacrificed, and the A498 tumors were weighed. Each *bar* represents the mean tumor weight and SE calculated for each treatment group. *P*s compared with saline: GTI-2040, $P < 0.0001$; scrambled, $P = 0.5145$; mismatched, $P = 0.5741$; 5-FU, $P = 0.9548$; vinblastine, $P = 0.0582$; and gemcitabine, $P = 0.0012$.

GTI-2040 Does Not Appear to Function via CpG-mediated Immune Stimulation. Although GTI-2040 has a CpG in its sequence, it is not in the optimal sequence context for either B-cell mitogen or NK activation (46, 47). Given that the antitumor effects are seen in SCID (T- and B-cell-deficient) mice, a significant CpG-mediated effect is not expected. In addition, CpG-mediated effects are not generally observed under conditions of systemic administration with saline as the vehicle. Furthermore, GTI-2040mismatched has a CpG in a similar sequence context to GTI-2040 but does not demonstrate efficacy in tumor growth, lymphoma survival, or metastasis assays (Figs. 5–9). Methylation of the C in the CpG dinucleotide does not abrogate GTI-2040-mediated antitumor activity, suggesting that the effect is not via CpG-mediated immune stimulation (data not shown). Finally, GTI-2040 treatment resulted in total regression of all tumors in SCID/beige mice, despite the lack of NK, B-cell, or T-cell function (Fig. 10). Taken together, these results suggest that the observed antitumor activity of GTI-2040 is not attributable to CpG-mediated immune stimulation. The experiments above were designed to address whether the antitumor activity of GTI-2040 is due to the sequence-specific down-regulation of *R2* mRNA and protein. These results do not rule out the possibility that immune stimulation may in fact contribute to the antitumor efficacy of GTI-2040 in immune-competent subjects. One argument against significant contributions from CpG-mediated effects is the observed lack of efficacy of the mismatched and scrambled controls against growth of R3 murine fibrosarcomas in immune-competent mice (Fig. 5). Future experiments may address the relative contributions of GTI-2040-mediated *R2* down-regulation and immune stimulation to the overall antitumor efficacy.

DISCUSSION

In the past decade, the approach to cancer treatment has evolved to reflect a growing understanding of the underlying mechanisms involved in the development and progression of the disease. There is a trend toward the discovery and development of drugs that specifically

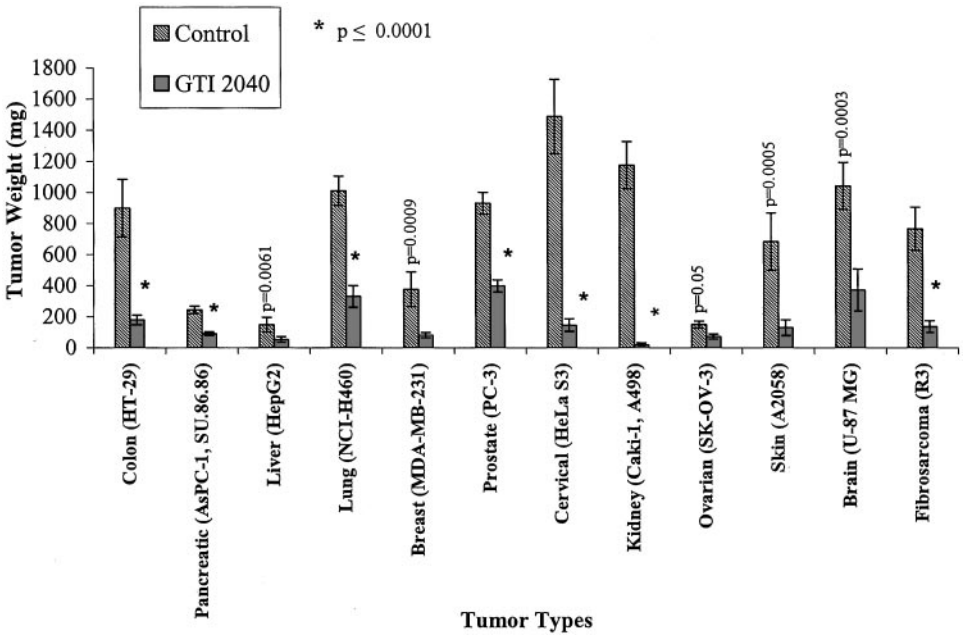

Fig. 7. The results of a number of human tumor xenograft experiments in mice are summarized. Each *data point* represents tumor weight and SE. Tumor cell suspensions (1.5×10^6 to 10^7) were injected s.c. into the right flank of the mice for the tumor lines shown, except for hepatocellular carcinoma cells, which were s.c. implanted as a tumor mass. Treatment started when a tumor mass was palpable. The tumor size usually ranged between 50 and 100 mm^3 before treatment. Oligonucleotide concentrations used in treatments ranged from 2.5 to 10 mg/kg, administered i.v., every second day. Tumor weight is expressed in mg and was obtained approximately 2 weeks after the start of oligonucleotide treatments, except for slow-growing tumors such as hepatocellular carcinoma, where tumor weight was obtained after 4 weeks of treatment. Differences in tumor weight between control and oligonucleotide-treated groups were statistically significant in all cases ($P < 0.05$).

target metabolic and signaling pathways that are unique to cells undergoing cellular transformation. Moreover, there is a trend toward disease management that recognizes the underlying mechanisms of disease progression to terminal stages. Inherent to these approaches is the promise of less invasive procedures and less toxic chemotherapeutic drugs. In addition to increased efficacy of treatment is the potential for a much higher quality of life for patients living with cancer.

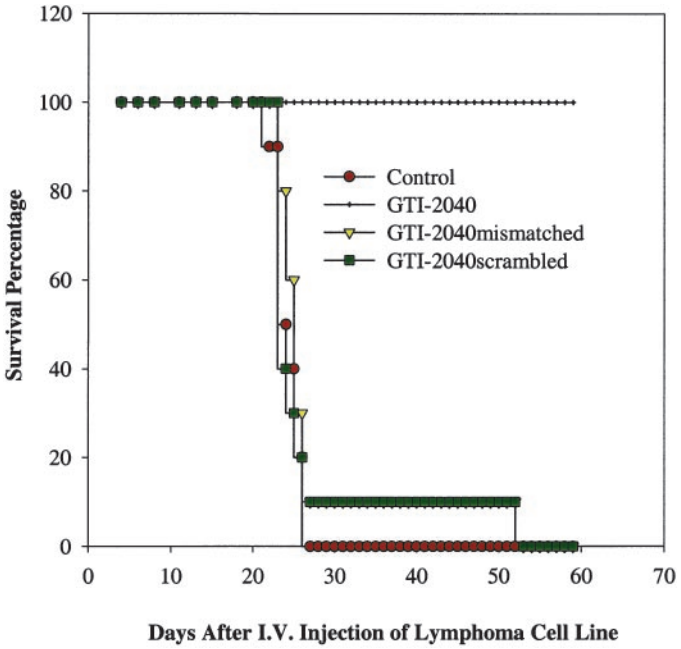

Fig. 8. Viable human Burkitt's lymphoma (Raji) cells (5×10^6) collected from subconfluent logarithmically growing cultures were injected i.v. into each animal, and disease was allowed to establish for 2 days. GTI-2040, GTI-2040scrambled, and GTI-2040mismatched, in normal saline, were administered by tail vein injection every second day at a dose of 10 mg/kg. At day 40, the treatment schedule was reduced to 10 mg/kg every 3 days. Control animals received saline alone, without ODN. Survival is presented as a percentage of the starting number of mice over time. All of the GTI-2040-treated mice survived to the end of the study and were sacrificed at day 72 due to animal housing limitations.

Antisense compounds, as a class, are uniquely suited to this emerging trend in cancer therapy in that they can be designed with exquisite specificity for a single target. Furthermore, the chemical modifications necessary to attain a reasonable pharmacokinetic profile and target cell uptake do not result in levels of toxicity observed with standard chemotherapeutic drugs (48–50). As a result, the limitation in the development of antisense therapeutics has been in the choice of target and not in the chemistry of the compounds.

It has become abundantly clear that cancer is not a disease with a single cause, and as a result, it is difficult to develop a single treatment that encompasses all cancer types. Antisense compounds that target cellular changes unique to a subset of cancers are in various stages of development. This approach can be successful if there is *a priori* evidence for the target being up-regulated in all cases of a given cancer type. An alternative approach to target selection is to find an underlying pathway that most if not all cancers converge upon in the process of growth and metastasis (*i.e.*, DNA replication and angiogenesis). Given that dNTP pools in a given cell are a limiting factor in DNA replication, it would be reasonable to hypothesize that decreasing the rate-limiting step in the production of dNTPs, *i.e.*, RNR, would have an overall antitumor effect in most tumor types. Further support for targeting RNR for antisense down-regulation is the previously reported increase in RNR activity in cancer cells. Apparently separate from its role in RNR, it has been demonstrated that R2 is directly involved in a number of signaling pathways that are essential to transformation. Both of the above observations suggest that R2 would be an excellent target for antisense down-regulation.

Essential to the development of an ODN as an antisense therapeutic is the demonstration that the mechanism of action is via direct and specific interaction with the target mRNA. Several criteria must be satisfied, both *in vitro* and *in vivo*, before it can be concluded that an ODN has bioactivity attributable to an antisense mechanism of action (51). Screening of 102 ODNs complementary to *R2* mRNA resulted in the choice of GTI-2040 as a lead antisense compound. The data presented here are consistent with the conclusion that the antitumor activity of GTI-2040 is via antisense-mediated down-regulation of R2. First, the *in vitro* data clearly demonstrate that GTI-2040 specifically targets the R2 subunit of RNR, resulting in down-regulation of both mRNA and protein (Fig. 2). Control ODNs were ineffective at down-

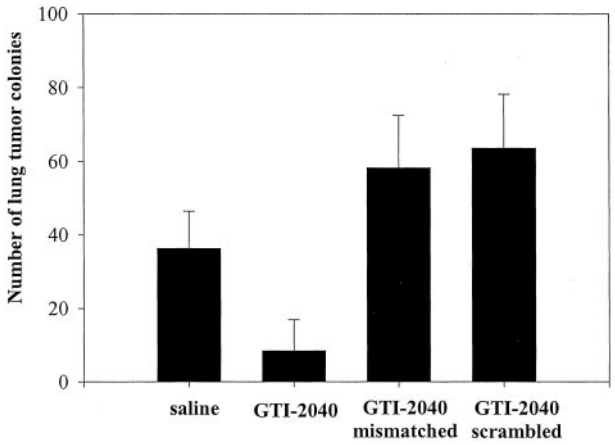

Fig. 9. C8161 human metastatic melanoma cells were seeded into 100-mm tissue culture dishes at a density of 2×10^6 cells/dish and incubated overnight at 37°C in α-MEM supplemented with 10% FBS. The cells were trypsinized and collected by centrifugation, and aliquots were removed from the suspension to determine the cell viability using the trypan blue exclusion test. Approximately 1×10^5 cells suspended in 0.1 ml of PBS were injected into the tail veins of 6–8-week-old female SCID mice. Treatment, as described in the Fig. 8 legend, was initiated after 2 days. Estimates of the number of lung nodules were made 5–7 weeks later, after excised lungs from individual mice were stained with picric acid dye solution (75% picric acid, 20% formaldehyde, and 5% glacial acetic acid). The *bars* represent the mean number of nodules/mouse with SE. In the GTI-2040 treatment group, only one of the nine mice had lung nodules.

regulation, and nonspecific mRNA sequences were unaffected by GTI-2040 treatment (Figs. 2 and 4). Second, the decrease in *R2* levels in tumors (or spleens) isolated from mice treated with GTI-2040 supports the conclusion of an antisense mechanism *in vivo*. Taken together, these data fulfill three of the required criteria, target- and sequence-specific down-regulation and, by inference, intracellular targeting of the ODN (*i.e.*, *R2* mRNA levels decreased in isolated tumors, suggesting that targeting had occurred). Recently, GLP pharmacokinetic and toxicology studies were conducted as a requirement for entering Phase I clinical trials. Analyses of circulating GTI-2040 in rats and monkeys demonstrate that GTI-2040 stability, metabolism, and excretion are consistent with those of the class of phosphorothioate ODNs, thereby fulfilling the criteria of *in vivo* stability.[5] The control ODNs were not effective in any of the tumor models examined, reinforcing the conclusion that GTI-2040 acts via a sequence-specific antisense mechanism and that target down-regulation correlates with efficacy. This study did not address the rank-order potency criteria in characterization of GTI-2040. Without extensive pharmacokinetic, cellular uptake, and RNase H digestion analyses, it is impossible to draw sound conclusions as to rank-order potency, and as such, the issue was well beyond the scope of the current study.

One of the caveats of applying current antisense technology is the immunostimulatory properties of both the phosphorothioate-ODN backbone and CpG dinucleotides present in the sequence (44, 46, 47). The experiments presented here are not consistent with significant contributions of immune stimulation to GTI-2040-mediated anticancer activity. The effective concentrations and dosage schedules of GTI-2040 are higher than those reported for CpG-mediated effects (52). In addition, the mismatched control ODN, although retaining a CpG motif similar to that of GTI-2040, does not display any antitumor efficacy. Perhaps the best evidence for GTI-2040 activity via an antisense mechanism of action is the results of tumor growth assays in SCID/beige mice (Fig. 10). These mice lack NK, B-cell, and T-cell functions, and yet GTI-2040 has antitumor efficacy similar in kinetics and extent to similar experiments in SCID mice that retain NK function. Another caveat of using phosphorothioate ODNs comes from the polyanionic nature of these compounds, which results in high nonspecific serum protein binding. Whereas the control ODN results would suggest that nonspecific binding to serum proteins is not a significant factor in GTI-2040 antitumor activity, the possibility cannot be ruled out entirely. Alternatively, nonspecific binding to proteins may contribute to the toxicity profile of GTI-2040.

The data summarized in Fig. 7 demonstrate that GTI-2040 bioactivity was not limited to a subset of tumor types, consistent with the hypothesis that *R2* down-regulation would lead to antitumor effects across a broad spectrum of cancers. Another important factor in targeting RNR is that it need not be aberrantly expressed for down-regulation to have antitumor activity. Regardless of the initial RNR expression status (Fig. 1*a*), down-regulation will limit dNTP synthesis and, by extension, DNA synthesis required for tumor cell proliferation and tumor growth. This is mirrored in the *in vivo* experiments, where both rapidly growing (colon, breast, and cervical) and slow-growing (pancreatic) tumors are effectively treated with GTI-2040. These properties make GTI-2040 unique among antisense drugs currently in development. Furthermore, GTI-2040 demonstrated efficacy against a number of aggressive cancers (lung cancer, pancreatic cancer, and lymphoma) for which there are limited treatment options. Although *R2* expression varied considerably among cancer cell lines (up to 10-fold) GTI-2040 was effective against all tumor xenografts. One explanation for this observation is that the 10 mg/kg/48 h dose is sufficient to down-regulate even the highest levels of *R2*, resulting in no difference in efficacy. Support for this possibility comes from a

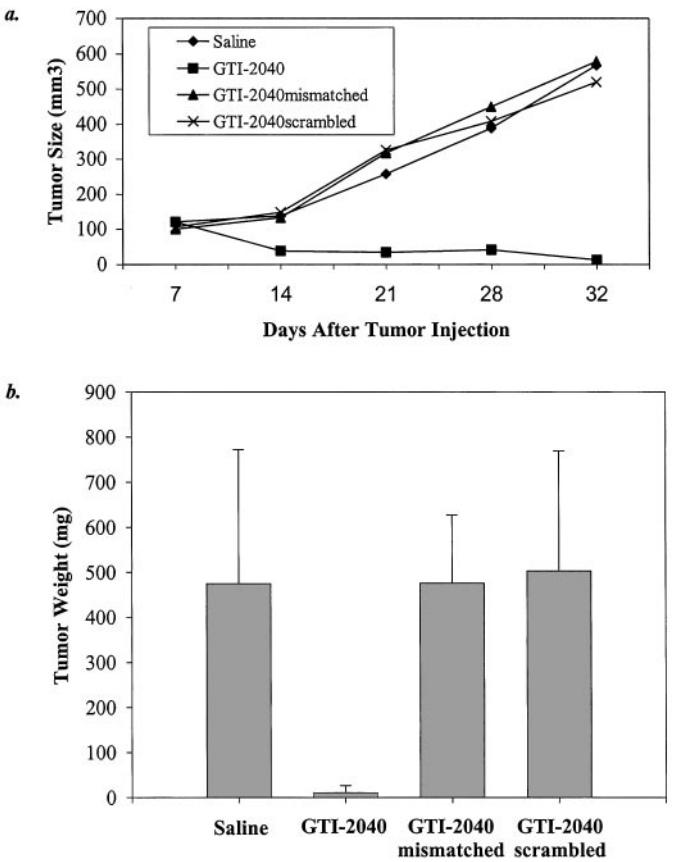

Fig. 10. The experiments with SCID/beige mice were essentially the same as those described for SCID mice (Fig. 6 legend). Each treatment group was composed of 10 mice, and the *data points* reflect the mean of each treatment group. *a*, caliper measurements at 1-week intervals were used to calculate tumor volumes. Each *point* represents mean tumor volume calculated from 10 animals/experiment. *P*s compared with saline: GTI-2040, $P < 0.0001$; scrambled, $P = 0.7076$; and mismatched, $P = 0.4186$. *b*, after 32 days, the mice were sacrificed, and the tumors were weighed. Each *bar* represents the mean tumor weight and SE calculated for each treatment group. *P*s compared with saline: GTI-2040, $P < 0.0001$; scrambled, $P = 0.7327$; and mismatched, $P = 0.9903$.

study by Miraglia *et al.* (53). This study demonstrated that *in vitro* target down-regulation by antisense compounds does not correlate with mRNA copy number (53). The IC_{50} of several antisense compounds was relatively constant, irrespective of the mRNA content (1 to >100 copies; Ref. 53). An alternative explanation is based on the observation that the proliferative rate of tumor cells in culture varies dramatically from that of the same tumor cells xenografted into mice (54). As a result, it is difficult to predict the level of RNR enzymatic activity that will be required by tumor cells under different growth environments. Although it is not always possible to extrapolate *in vitro* result to *in vivo*, the results would indicate that GTI-2040 is effective across a broad range of *R2* expression. This is an important observation, given the complexity of R2 expression that might be predicted for patients in the clinical setting.

The excellent efficacy of GTI-2040 in *in vivo* tumor growth, metastasis, and survival assays underscores the therapeutic potential of targeting RNR, and taken together, these data demonstrate the importance of targeting pathways common to the process of transformation. A strong argument for the further development of GTI-2040 is its superior efficacy compared with standard chemotherapeutic drugs that are known to target the same pathway. In many cases, chemotherapeutic drugs are limited due to a lack of specificity that leads to pleiotropic effects and toxicity at doses lower than those required for optimal target inhibition. This does not appear to be the case with GTI-2040. GLP toxicology studies in rats and monkeys have been completed, and the results are consistent with GTI-2040 being safe at clinically relevant dosages.[5] A Phase I trial of GTI-2040 has recently been completed, and GTI-2040 was well tolerated.[6] Given the favorable safety profile of GTI-2040 in Phase I clinical trial and the preclinical efficacy against a broad range of tumor types, preclinical animal studies were expanded to include assessment of GTI-2040 efficacy in combination with current therapeutic regimens.[7] Preliminary results have been highly promising and, as a result, have prompted a Phase II trial with GTI-2040 in combination chemotherapies. In conclusion, the results presented here support the development of GTI-2040 as a target-specific antisense therapeutic agent against a broad range of cancers.

ACKNOWLEDGMENTS

We thank Huaiyu Zhang for excellent technical assistance and members of Lorus Therapeutics Inc. for helpful discussions and critical reading of the manuscript.

REFERENCES

1. Cory, J. G. Purine and pyrimidine nucleotide metabolism. *In:* T. Devlin (ed.) Biochemistry with Clinical Correlations, 4th ed., pp. 489–523. New York: Wiley-Liss, 1997.
2. Tonin, P. N., Stallings, R. L., Carman, M. D., Bertino, J. R., Wright, J. A., Srinivasan, P. R., and Lewis, W. H. Chromosomal assignment of amplified genes in hydroxyurea-resistant hamster cells. Cytogenet. Cell Genet., *45:* 102–108, 1987.
3. Engstrom, Y., Eriksson, S., Jildevik, I., Skog, S., Thelander, L., and Tribukait, B. Cell cycle-dependent expression of mammalian ribonucleotide reductase. J. Biol. Chem., *260:* 9114–9116, 1985.
4. Nocentini, G. Ribonucleotide reductase inhibitors: new strategies for cancer chemotherapy. Crit. Rev. Oncol. Hematol., *22:* 89–126, 1996.
5. Chabes, A., and Thelander, L. Controlled protein degradation regulates ribonucleotide reductase activity in proliferating mammalian cells during the normal cell cycle and in response to DNA damage and replication blocks. J. Biol. Chem., *275:* 17747–17753, 2000.
6. Albert, D. A., and Rozengurt, E. Synergistic and coordinate expression of the genes encoding ribonucleotide reductase subunits in Swiss 3T3 cells: effect of multiple signal-transduction pathways. Proc. Natl. Acad. Sci. USA, *89:* 1597–1601, 1992.
7. Albert, D. A., and Nodzenski, E. Ribonucleotide reductase gene expression during cyclic AMP-induced cell cycle arrest in T lymphocytes. Exp. Cell Res., *203:* 476–482, 1992.
8. Albert, D. A., and Rozengurt, E. Opposite effects of cyclic AMP on the expression of the genes encoding ribonucleotide reductase in Swiss 3T3 and RAT 1 cells. Biochem. Biophys. Res. Commun., *196:* 642–649, 1993.
9. Fredriksson, J. M., and Nedergaard, J. Norepinephrine specifically stimulates ribonucleotide reductase subunit R2 gene expression in proliferating brown adipocytes: mediation via a cAMP/PKA pathway involving Src and Erk1/2 kinases. Exp. Cell Res., *274:* 207–215, 2002.
10. Tanaka, H., Arakawa, H., Yamaguchi, T., Shiraishi, K., Fukuda, S., Matsui, K., Takei, Y., and Nakamura, Y. A ribonucleotide reductase gene involved in a *p53*-dependent cell-cycle checkpoint for DNA damage. Nature (Lond.), *404:* 42–49, 2000.
11. Nakano, K., Balint, E., Ashcroft, M., and Vousden, K. H. A ribonucleotide reductase gene is a transcriptional target of *p53* and *p73*. Oncogene, *19:* 4283–4289, 2000.
12. Yamaguchi, T., Matsuda, K., Sagiya, Y., Iwadate, M., Fujino, M. A., Nakamura, Y., and Arakawa, H. p53R2-dependent pathway for DNA synthesis in a *p53*-regulated cell cycle checkpoint. Cancer Res., *61:* 8256–8262, 2001.
13. Guittet, O., Hakansson, P., Voevodskaya, N., Fridd, S., Graslund, A., Arakawa, H., Nakamura, Y., and Thelander, L. Mammalian p53R2 protein forms an active ribonucleotide reductase *in vitro* with the R1 protein, which is expressed both in resting cells in response to DNA damage and in proliferating cells. J. Biol. Chem., *276:* 40647–40651, 2001.
14. Crenshaw, T. R., and Cory, J. G. Overexpression of protein disulfide isomerase-like protein in a mouse leukemia L1210 cell line selected for resistance to 4-methyl-5-amino-1-formylisoquinoline thiosemicarbazone, a ribonucleotide reductase inhibitor. Adv. Enzyme Regul., *42:* 143–157, 2002.
15. Green, D. A., Antholine, W. E., Wong, S. J., Richardson, D. R., and Chitambar, C. R. Inhibition of malignant cell growth by 311, a novel iron chelator of the pyridoxal isonicotinoyl hydrazone class: effect on the R2 subunit of ribonucleotide reductase. Clin. Cancer Res., *7:* 3574–3579, 2001.
16. Gao, Y., Liehr, S., and Cooperman, B. S. Affinity-driven selection of tripeptide inhibitors of ribonucleotide reductase. Bioorg. Med. Chem. Lett., *12:* 513–515, 2002.
17. Fagny, C., Vandevelde, M., Svoboda, M., and Robberecht, P. Ribonucleotide reductase and thymidine phosphorylation: two potential targets of azodicarbonamide. Biochem. Pharmacol., *64:* 451–456, 2002.
18. Feun, L., Modiano, M., Lee, K., Mao, J., Marini, A., Savaraj, N., Plezia, P., Almassian, B., Colacino, E., Fischer, J., and MacDonald, S. Phase I and pharmacokinetic study of 3-aminopyridine-2-carboxaldehyde thiosemicarbazone (3-AP) using a single intravenous dose schedule. Cancer Chemother. Pharmacol., *50:* 223–229, 2002.
19. Angus, S. P., Wheeler, L. J., Ranmal, S. A., Zhang, X., Markey, M. P., Mathews, C. K., and Knudsen, E. S. The retinoblastoma tumor suppressor targets dNTP metabolism to regulate DNA replication, J. Biol. Chem., *277:* 44376–44384, 2002.
20. Fan, H., Villegas, C., Huang, A., and Wright, J. A. The mammalian ribonucleotide reductase R2 component cooperates with a variety of oncogenes in mechanisms of cellular transformation. Cancer Res., *58:* 1650–1653, 1998.
21. Fan, H., Villegas, C., and Wright, J. A. Ribonucleotide reductase R2 component is a novel malignancy determinant that cooperates with activated oncogenes to determine transformation and malignant potential. Proc. Natl. Acad. Sci. USA, *93:* 14036–14040, 1996.
22. Huang, A., Fan, H., Taylor, W. R., and Wright, J. A. Ribonucleotide reductase *R2* gene expression and changes in drug sensitivity and genome stability. Cancer Res., *57:* 4876–4881, 1997.
23. Goan, Y. G., Zhou, B., Hu, E., Mi, S., and Yen, Y. Overexpression of ribonucleotide reductase as a mechanism of resistance to 2,2-defluorodeoxycytidine in the human KB cancer cell line. Cancer Res., *59:* 4204–4207, 1999.
24. Zhou, B. S., Hsu, N. Y., Pan, B. C., Doroshow, J. H., and Yen, Y. Overexpression of ribonucleotide reductase in transfected human KB cells increases their resistance to hydroxyurea: *M2* but not *M1* is sufficient to increase resistance to hydroxyurea in transfected cells. Cancer Res., *55:* 1328–1333, 1995.
25. Chen, S., Zhou, B., He, F., and Yen, Y. Inhibition of human cancer cell growth by inducible expression of human ribonucleotide reductase antisense cDNA. Antisense Nucleic Acid Drug Dev., *10:* 111–116, 2000.
26. Kuschak, T. I., Kuschak, B. C., Taylor, C. L., Wright, J. A., Wiener, F., and Mai, S. c-Myc initiates illegitimate replication of the ribonucleotide reductase *R2* gene. Oncogene, *21:* 909–920, 2002.
27. Opalinska, J. B., and Gewirtz, A. M. Nucleic-acid therapeutics: basic principles and recent applications. Nat. Rev. Drug Discov., *1:* 503–514, 2002.
28. Braasch, D. A., and Corey, D. R. Novel antisense and peptide nucleic acid strategies for controlling gene expression. Biochemistry, *41:* 4504–4510, 2002.
29. Flaherty, K. T., Stevenson, J. P., and O'Dwyer. P. J. Antisense therapeutics: lessons from early clinical trials. Curr. Opin. Oncol., *13:* 499–505, 2001.
30. Field, A. K., and Goodchild, J. Antisense oligonucleotides: rational drug design for genetic pharmacology. Exp. Opin. Investig. Drugs, *4:* 799–821, 1995.
31. Dolnick, B. J. Antisense agents in cancer research and therapeutics. Cancer Invest., *9:* 185–194, 1991.
32. Welch, D. R., Bisi, J. E., Miller, B. E., Conaway, D., Seftor, E. A., Yohem, K. H., Gilmore, L. B., Seftor, R. E., Nakajima, M., and Hendrix, M. J. Characterization of a highly invasive and spontaneously metastatic human malignant melanoma cell line. Int. J. Cancer, *47:* 227–237, 1991.
33. Choy, B. K., McClarty, G. A., Chan, A. K., Thelander, L., and Wright, J. A. Molecular mechanisms of drug resistance involving ribonucleotide reductase: hy-

[6] L. Janisch, A. A. Desai, W. M. Stadler, N. J. Vogelzang, M. J. Ratain, S. Z. Cadden, A. H. Young, R. L. Schilsky. Phase I study of GTI-2040 given by continuous intravenous infusion (CVI) in patients with advanced malignancies, manuscript in preparation.

[7] A. Vassilakos, Y. Lee, N. Feng, K. Xiong, M. Wang, H. Jin, J. Wright, A. Young. Enhanced antitumor efficacy of GTI-2040 in combination with standard chemotherapy, manuscript in preparation.

droxyurea resistance in a series of clonally related mouse cell lines selected in the presence of increasing drug concentrations. Cancer Res., *48:* 2029–2035, 1988.
34. Mann, G. J., Graslund, A., Ochiai, E., Ingemarson, R., and Thelander, L. Purification and characterization of recombinant mouse and herpes simplex virus ribonucleotide reductase R2 subunit. Biochemistry, *30:* 1939–1947, 1991.
35. Chan, A. K., Litchfield, D. W., and Wright, J. A. Phosphorylation of ribonucleotide reductase R2 protein: *in vivo* and *in vitro* evidence of a role of p34cdc2 CDK2 protein kinases. Biochemistry, *32:* 12835–12840, 1993.
36. Bhatia, P., Taylor, W. R., Greenberg, A. H., and Wright, J. A. Comparison of glyceraldehyde-3-phosphate dehydrogenase and 28S-ribosomal RNA gene expression as RNA loading controls for Northern blot analysis of cell lines of varying malignant potential. Anal. Biochem., *216:* 223–226, 1994.
37. McClarty, G. A., Chan, A. K., Engstrom, Y., Wright, J. A., and Thelander, L. Elevated expression of *M1* and *M2* components and drug-induced posttranslational modulation of ribonucleotide reductase in a hydroxyurea-resistant mouse cell line. Biochemistry, *26:* 8004–8011, 1987.
38. Wright, J. A., Alam, T. G., McClarty, G. A., Tagger, A. Y., and Thelander, L. Altered expression of ribonucleotide reductase and role of *M2* gene amplification in hydroxyurea-resistant hamster, mouse, rat, and human cell lines. Somatic Cell Mol. Genet., *13:* 155–165, 1987.
39. Thelander, L., and Berg, P. Isolation and characterization of expressible cDNA clones encoding the *M1* and *M2* subunits of mouse ribonucleotide reductase. Mol. Cell. Biol., *6:* 3433–3442, 1986.
40. Pavloff, N., Rivard, D., Masson, S., Shen, S., and Mes-Masson, A. Sequence analysis of the large and small subunits of human ribonucleotide reductase. DNA Seq., *2:* 227–234, 1992.
41. Takeda, E., and Weber, G. Role of ribonucleotide reductase in expression of the neoplastic program. Life Sci., *28:* 1007–1014, 1981.
42. Jensen, R. A., Page, D. L., and Holt, J. T. Identification of genes expressed in premalignant breast disease by microscopy-directed cloning. Proc. Natl. Acad. Sci. USA, *91:* 9257–9261, 1994.
43. Saeki, T., Takashima, S., Ohsumi, S., Saeki, H., Takiyama, W., Kurita, A., and Yokoyama, N. Ribonucleotide reductase highly expressed in breast cancer patients with hormone receptors. Proc. Am. Soc. Clin. Oncol., 1997.
44. Monteith, D. K., Henry, S. P., Howard, R. B., Flournoy, S., Levin, A. A., Bennett, F., and Crooke, S. T. Immune stimulation: a class effect of phosphorothioate oligodeoxynucleotides in rodents. Anti-Cancer Drug Design, *12:* 421–432, 1997.
45. Frenkel, G. D., and Caffrey, P. B. A prevention strategy for circumventing drug resistance in cancer chemotherapy. Curr. Pharm. Des., *7:* 1595–1614, 2001.
46. Krieg, A. M. Immune effects and mechanisms of action of CpG motifs. Vaccine, *19:* 618–622, 2001.
47. Krieg, A. M. CpG motifs in bacterial DNA and their immune effects. Annu. Rev. Immunol., *20:* 709–760, 2002.
48. Agrawal, S., and Akhtar, S. Advances in antisense efficacy and delivery. Trends Biotechnol., *13:* 197–199, 1995.
49. Akhtar, S., Hughes, M. D., Khan, A., Bibby, M., Hussain, M., Nawaz, Q., Double, J., and Sayyed, P. The delivery of antisense therapeutics. Adv. Drug Deliv. Rev., *44:* 3–21, 2000.
50. Dokka, S., and Rojanasakul, Y. Novel non-endocytic delivery of antisense oligonucleotides. Adv. Drug Deliv. Rev., *44:* 35–49, 2000.
51. Crooke, S. T. Proof of mechanism of antisense drugs. Antisense Nucleic Acid Drug Dev., *6:* 145–147, 1996.
52. Whitmore, M. M., Li, S., Falo, L., Jr., and Huang, L. Systemic administration of LPD prepared with CpG oligonucleotides inhibits the growth of established pulmonary metastases by stimulating innate and acquired antitumor immune response. Cancer Immunol. Immunother., *50:* 503–514, 2001.
53. Miraglia, L., Watt, A. T., Graham, M. J., and Crooke, S. T. Variations in mRNA content have no effect on the potency of antisense oligonucleotide. Antisense Nucleic Acid Drug Dev., *10:* 453–461, 2000.
54. Hayflick, L. Mortality and immortality at the cellular level: a review. Biochemistry, *62:* 1180–1190, 1997.

GTI-2040, an Antisense Agent Targeting the Small Subunit Component (R2) of Human Ribonucleotide Reductase, Shows Potent Antitumor Activity against a Variety of Tumors

Yoon Lee, Aikaterini Vassilakos, Ningping Feng, et al.

Cancer Res 2003;63:2802-2811.